Science Advances

AAAS

advances.sciencemag.org/cgi/content/full/4/6/eaar4206/DC1

Supplementary Materials for

Nanophotonic particle simulation and inverse design using artificial neural networks

John Peurifoy, Yichen Shen, Li Jing, Yi Yang, Fidel Cano-Renteria, Brendan G. DeLacy, John D. Joannopoulos, Max Tegmark, Marin Soljačić

Published 1 June 2018, *Sci. Adv.* **4**, eaar4206 (2018)
DOI: 10.1126/sciadv.aar4206

This PDF file includes:

I. SUPPLEMENTALS

section S1. Details for the comparison of NNs with inverse design algorithms

This section describes the results and details involved in comparing the inverse design runtimes.

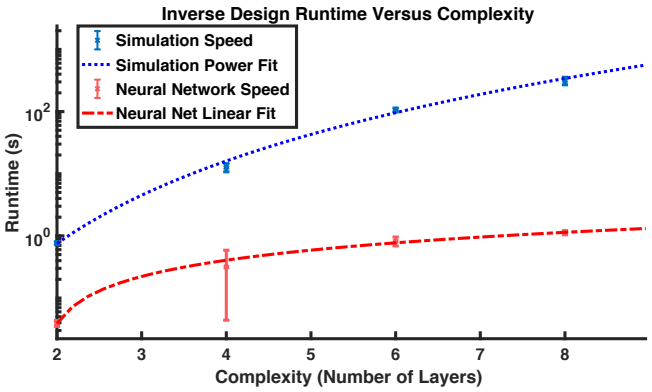

fig. S1. Comparison of inverse design runtime versus complexity of the nanoparticle. The runtime of the numerical optimization is seen to increase more quickly than that of the neural network. The simulation is fit with a power fit (that finds an exponent of 4.5), and the neural network is fit with a linear fit.

To compare the runtime of the neural network versus the numerical methods, we first had to train the networks to a given error threshold as described above. To allow for approximately the same error threshold even as the particles became more complex, the size of the neural network was increased as we considered more complex particles. The two shell particle had 30,000 parameters, while the four shell had 46,000 and the six shell had 151,000. Note that equivalent performance may possibly be achieved with much fewer parameters, as these architectures were not heavily optimized.

To establish a robust and comparable 'accuracy cutoff' for the increasing complexity of the particles, we looked at the error rate of the numerical inverse design for the simulation. We did this because ultimately we wanted to perform a comparison of the neural network to the numerical inverse design on equal footing. Thus, we ensured that the neural network's accuracy cutoff during the training stage was below the error rate for the numerical inverse design. Effectively, we ran the numerical inverse design for five different particle configurations with the same number of shells, then found what the mean error rate of these tests were. This provided a robust and comparable 'accuracy cutoff' that we could then use to figure out what the size of the neural network should be for each nanoparticle.

To get an equal footing comparison — and trying to not bias our results to any particular choice of optimization method — the comparison described here used the same inverse design optimization function for both the neural network's and the simulation. The approach described in the paper, reverse-backpropogation, gives comparable results; however it is difficult to do a fair comparison due to different mediums and different algorithms. Thus, after experimenting with several optimization functions, we used the same function for both the simulation and neural network, simply adding in the analytical gradient for the case of the neural network — one of the key benefits.

The results of this are seen in Fig. 1. From these results, it is evident that the runtime of the simulation for inverse design becomes large, while the neural network can handle more complex problems in the equivalent speed. The difference in the scaling — the power fit for the simulation versus the linear fit of the neural network — is one of the promising features about using this method.

section S2. J aggregates

Nanoparticles made from J-Aggregates often consist of a core shell geometry (normally made of a metal), surrounded by a shell of dielectric material, and then coated with a J-Aggregate dye. This dye is peculiar because it couples with the metallic core to produce exciton resonance structures. These materials have allowed advanced studies of plasmon-exciton interactions and have been used to generate phenomena like induced transparency. These materials are powerful because the scientist can choose where these resonance structures and peaks happen in the material, and as such offer a level of customizability in designing nanoparticles.

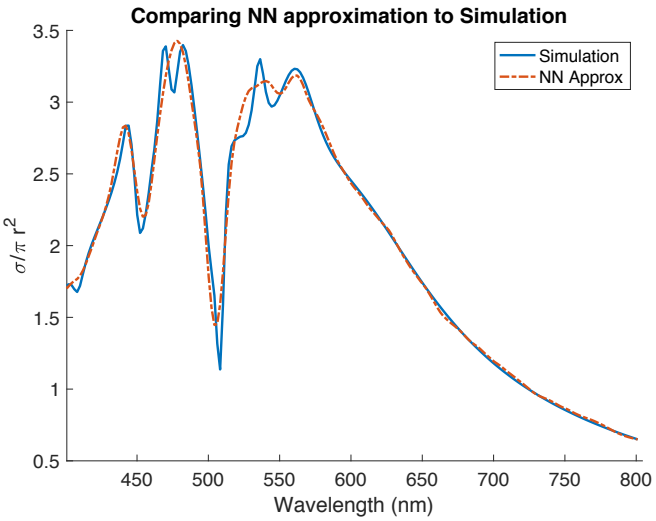

fig. S2. Comparison of NN approximation to the real spectrum for a particle made with a J-aggregate material. The sharp peak in the spectrum is due to a resonance phenomenon in the J-Aggregate material, and can be customized for a variety of wavelengths. This result was generated from a particle not seen in the training data.

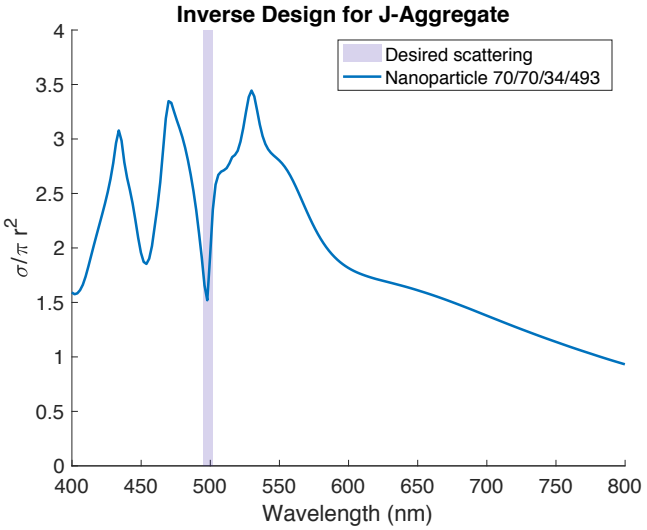

fig. S3. Optimization of scattering at a particular wavelength using the J-aggregate material. The sharp peaks in the result are possible due to the material properties of J-aggregates, and present a complex scattering behavior.

This customizability — which often can drastically change the spectra produced by these particles — is a feature that makes these nanoparticles good litmus tests for the robustness of the network.

Here we considered a three shell particle made of a metallic silver core, a dielectric shell of silica, and an outside shell of J-Aggregate dye. Each shell ranged from 30nm-70nm, and the J-Aggregate dye had a different dielectric function for each training example. The frequency-dependent dielectric ϵ function of the J-Aggregate dye was given by:

$$\epsilon(\omega) = \epsilon_0 + \frac{f\omega_0^2}{\omega_0^2 - \omega^2 - i\gamma\omega} \tag{1}$$

Where $\epsilon_0 = 1.85$, $f = 1.0$, $\gamma = .01$, $\omega = \frac{2\pi}{\lambda}$. To control the value of this dielectric constant, λ_d was varied in $\omega_0 = \frac{2\pi}{\lambda_d}$ between 400 to 700nm. Note that this tunes the location of the resonance peak, but not the width of the peak.

By varying the dielectric function, this means that each training example was different and had peaks located at significantly different locations. The inputs were only the thickness of each shell and the resonance peak of the J-Aggregate material, no other information was supplied to the network.

Following the same procedure as above, the results of the network were visually inspected by testing a spectrum that had not been trained on — Fig. 2. Results demonstrated that despite the spectra being different due to the changed resonance peak, the network was robust and could still approximate well.

Similarly, we performed inverse design with J-Aggregates — Fig. 3. Due to the J-aggregate material, the sample space of spectra was much broader, and thus the results from the network were more attuned for the optimization. The sharper peaks allowed the network to find much more optimal configurations of the particle.

These results demonstrate that the network is robust even with sharp features in the spectrum, and furthermore that even with large sample spaces, the network is able to function as an optimization tool and create unique geometries.